Journal of Power Sources 262 (2014) 213–218

Contents lists available at ScienceDirect

Journal of Power Sources

journal homepage: www.elsevier.com/locate/jpowsour

Construction of porous anode by sacrificial template for a passive direct methanol fuel cell

Qinghong Huang [a,b], Jingjing Jiang [b], Jieshi Chai [b], Ting Yuan [b], Haifeng Zhang [b,*], Zhiqing Zou [b], Xiaogang Zhang [a], Hui Yang [b,*]

[a] College of Material Science and Engineering, Nanjing University of Aeronautics and Astronautics, Nanjing 210016, China
[b] Center for Energy Storage and Conversion, Shanghai Advanced Research Institute, Chinese Academy of Sciences, Shanghai 201210, China

HIGHLIGHTS

- MgO nanoparticles are used as a sacrificial template to construct the porous anode.
- The DMFC with porous anode exhibits a significant increase in catalyst utilization.
- The DMFC with 50% reduced anode catalyst loading exhibits an enhanced performance.

ARTICLE INFO

Article history:
Received 23 January 2014
Received in revised form
7 March 2014
Accepted 24 March 2014
Available online 3 April 2014

Keywords:
Sacrificial pore-former
Anodic porous structure
Catalyst utilization
Membrane electrode assembly
Direct methanol fuel cell

ABSTRACT

Simple addition of magnesium oxide (MgO) nanoparticles as a sacrificial pore-former into the catalytic layer (CL) and micro-porous layer (MPL) in the anode of a membrane electrode assembly (MEA) leads to the formation of porous anodic structure, thus greatly enhancing the performance of a passive direct methanol fuel cell. At the same PtRu(1:1) loading of 2.0 mg cm^{-2}, the MEAs with porous CL and with both porous MPL and CL exhibit the maximal power densities of 37.0 and 43.7 mW cm^{-2} at a temperature of 25 °C and with 3 M of methanol solution, respectively. When the PtRu loading decreases to 1.0 mg cm^{-2}, the maximum power density of an MEA with both porous MPL and CL is ca. 32.8 mW cm^{-2}, which is even higher than that of a conventional MEA with a PtRu loading of 2.0 mg cm^{-2}. The improved performance of the novel MEA can be ascribed to an increased electrochemical surface area, a decreased charge-transfer resistance as well as an efficient mass transfer of methanol after the formation of porous structure in the anode. The present work provides a very simple but very effective way to reduce the dosage of the noble metal catalysts for fuel cells.

1. Introduction

The passive direct methanol fuel cell (DMFC) is very suitable as power for portable electronic devices due to its high energy density, system simplicity and ambient operation conditions [1,2]. The performance of a passive DMFC strongly depends on the structure and property of a membrane electrode assembly (MEA), where the electrochemical reactions take place. An MEA typically consists of a membrane, two micro-porous layers (MPLs) and two catalytic layers (CLs). The MPLs consist of hydrophobic pores and carbon particles, facilitating the diffusion of both fuel and gas, as well as the removal of reaction products [3–6]. The CLs are critical for the performance improvement of an MEA because the oxidation and reduction reactions occur on catalyst particles distributed on CLs. Recently, extensive research efforts have been focused on the improvement of the structure and composition of the MEAs [7–12], so as to promote their performance and to reduce the noble metal loading within a DMFC.

It is reported that during DMFC operations, a complex flow of reactants and reaction products exists in pores of the electrodes [13]. Therefore, the construction of a layer with novel morphology and pore structure that is tailored to meet the best performance of a DMFC is very important. Several groups have reported the positive effects of porous cathodic CLs on DMFC performance. The morphology and pore structure of cathodic CLs can be optimized by fabrication methods [14] or by addition of pore forming agents such as: (i) organic compounds; which can be easily removed by sublimation or other treatments [15,16]; (ii) low-temperature decomposable inorganic substances, which can be removed during drying

* Corresponding authors. Fax: +86 21 20325112.
E-mail addresses: zhanghf@sari.ac.cn (H. Zhang), yangh@sari.ac.cn, huiyang65@hotmail.com (H. Yang).

http://dx.doi.org/10.1016/j.jpowsour.2014.03.121
0378-7753/

or hot-pressing. These components generally refer to amines, such as NH_4HCO_3, $(NH_4)_2CO_3$, $(NH_4)_2C_2O_4$, etc. [17–19]; (iii) carbon materials, which have filamentous or porous morphology. They remain in the CLs to increase the porosity of electrodes [13,20,21]. (iv) metal oxides or salts ($MgSO_4$, SiO_2, etc.), which can be dissolved by acid, base or boiled deionized water [22,23]. Lee et al. [23] recently investigated the effects of porosity within the CLs using SiO_2 as a pore-former, and the results showed that the pores in cathodic CLs lead to a DMFC performance promotion by 55.5%.

In spite of many reports that focused on porous cathodic CLs, however, for a passive DMFC, the MEA performance is usually restricted by the anodic structure because of its slow anodic reaction kinetics [24] and the lack of fuel supplement to the catalytic layer [25,26]. Therefore, it is also crucial to design the pore structure of anode for better DMFC performance. The anodic pores, typically including the pores in anodic MPLs and CLs, play an important role in promoting an efficient transport of methanol from fuel reservoir to the catalyst surface [27]. The control of porosity in the CLs can also help to increase the electrochemical surface area (ECSA) of the electrodes by optimizing the triple-phase boundaries in the CLs. For example, Yang et al. [28] found that the addition of carbon nanotubes in the anodic MPLs significantly improves the MEA performance by enhancing both mass transfer of methanol and catalyst utilization. Recent work by A.S. Bauskar et al. [29] indicated that the maximum power density of a fuel cell increased by 25% while using Li_2CO_3 as an anodic pore-former. However, few works focus on an investigation of the influence of pores distributed in different layers of anodes on the passive DMFC's performance.

In this work, we report a simple addition of magnesium oxide (MgO) nanoparticles as a sacrificial pore-former into CL and MPL in the anode of an MEA for a passive DMFC. MgO nanoparticles as sacrificial template would be preferential pore-forming agent because the size, volume and distribution of the pores within the electrodes could be controlled that might provide a possibility for construction of an optimized or even ordered nanostructured anode. After the formation of an MEA, MgO nanoparticles can be easily dissolved and removed by washing with acidic solution. The relationship between MgO content and DMFC's performance will be investigated. It was found that the addition of MgO nanoparticles as sacrificial template leads to the formation of porous anodic structure, thus greatly improving the performance of a passive DMFC.

2. Experimental

2.1. Preparation of an MEA

The Nafion 115 membrane was sequentially cleaned in 3 vol. % H_2O_2, 0.5 M H_2SO_4, and de-ionized water at 80 °C for 2 h. To prepare the MPL, a slurry which consists of a mixture of carbon powder (Vulcan® XC-72R) and 20 wt. % PTFE was well-dispersed and sprayed onto the wet-proofed Toray® carbon paper (TGPH-60, Toray Inc.) via an automatic dispenser. XC-72R carbon loadings for the cathodic and anodic MPLs are ca. 2.0 and 1.0 mg cm^{-2}, respectively. For the formation of porous MPL, MgO nanoparticles with an average diameter of ca. 50 nm (Aladdin Industrial Corporation) were added into above slurry before dispersion.

The electrocatalysts used in this work are the mixture of Pt–Ru (1:1) black and 40 wt. % Pt-20 wt.% Ru/C for the anode, Pt black and 60 wt.% Pt/C for the cathode, respectively. The mass ratio between unsupported and carbon-supported catalysts is 1:1.67 for both the anode and cathode. The catalyst ink was prepared by dispersing the appropriate amount of catalysts and 5 wt. % Nafion solution (Aldrich) into a mixture of isopropyl alcohol and ultrapure water with a volume ratio of 1:1. The Nafion ionomer loading is 20 wt. % in the catalyst ink both for the cathode and anode. The catalyst ink was then blade-coated on the as-prepared MPL. For the formation of porous CL, MgO nanoparticles were added into above ink before dispersion. Unless stated otherwise, the noble metal loadings for the anode and cathode of the MEAs are 2.0 and 4.0 mg cm^{-2}, respectively.

Finally, a well-treated Nafion 115 membrane was sandwiched between the two electrodes by hot-pressing at 130 °C and 6 MPa for 3 min to form an MEA with an active geometric area of 4 cm^2. To remove MgO nanoparticles, the as-prepared MEAs were immersed into a 0.5 M H_2SO_4 aqueous solution overnight. The solution was mildly stirred by a magnetic stirrer which was separated from the MEAs through a plastic filter. Then, the MEAs were rinsed with deionized water thoroughly. The residual Mg^{2+} ions in the secondary acid leaching solution are not detected through inductively coupled plasma spectrometry (ICP), confirming that a single acid-leaching process overnight can lead to a complete removal of MgO particles.

2.2. Surface morphology of the anodes

Surface morphology of the anodes was characterized by scanning electron microscopy (SEM) using Hitachi S-4700 microscope operated at an accelerating voltage of 10.0 kV.

2.3. Single DMFC test

All the tests were conducted at a temperature of ca. 25 °C and with a relative humidity (RH) of ca. 30%. Prior to testing, the MEA was activated under ambient condition by immersing into 2 M methanol solution for 24 h. The MEA was sandwiched between two Au-deposited stainless steel plates with open areas of ca. 75% for the anode and cathode. Air and fuel were supplied to the electrodes only by self-diffusion through the open areas. The polarization curves of the passive DMFCs were obtained with 3 M of methanol solution on an Arbin FCT testing system (Arbin Instrument Inc., USA). For each discharging current point along the polarization curve, a period of 2 min as waiting time was maintained to obtain a steady voltage. In our tests, for each MEA, all the polarization curves were acquired for three times, and the standard deviation of the maximum power density values calculated from polarization curves in repeated tests are basically less than 1.5 mW cm^{-2}.

2.4. Electrochemical characterizations

The cyclic voltammetric (CV) measurements were carried out with Solartron SI1287 Potentiostat/Galvanostat to characterize the ECSAs of the anodes of the MEAs by feeding the water to the anode of a DMFC as the working electrode, humidified H_2 to the cathode at a flow rate of about 5 mL min^{-1} as the counter electrode and dynamic hydrogen electrode (DHE). The working potential was cycled between 0 and 0.76 V at a scan rate of 20 mV s^{-1}.

Electrochemical impedance spectra (EIS) were recorded using a Solartron SI2610 controlled by a personal computer and coupled to a Solartron SI1287 Potentiostat/Galvanostat. All the anode impedance spectra recorded were measured between anode and DHE at the cathode, and the overpotential of the DHE is negligible according to the previous work [30]. Impedance spectra were obtained in a frequency range between 100 kHz and 0.01 Hz at a given potential of 0.40V/DHE, and the amplitude of the sinusoidal voltage signal is 10 mV. During all the electrochemical measurements, the cells were placed in a thermostated container at a temperature of ca. 25 ± 1 °C.

3. Results and discussion

Fig. 1 shows the surface morphologies of conventional MPL and CL, and porous anodic MPL and CL after removal of 20 wt. % MgO nanoparticles. As seen from SEM images, the surface of conventional anodic MPL and CL are generally even and compact, containing calcareous-sponge-shaped particles and some small interparticle pores. The small interparticle pores are formed by solvent evaporation during the preparation of the anodic MPL and CL. For a comparison, the surface of porous anodic MPL and CL are more rough and loose. Importantly, the inter-particle pores with the size of about 200–500 nm, formed by the removal of MgO particles are larger than that of conventional MPL and CL. These pores exist as either independent or interlaced aggregations, which might lead to an improvement in both catalyst utilization and mass transportation in the anode. We have also conducted SEM and BET measurements on porous MPLs and CLs after removal of different contents of MgO particles, no obvious differences are observed, probably due to the formation of interconnected pores after the removal of MgO.

Fig. 2(A) shows the polarization curves of the passive DMFCs with porous anodic CLs after removal of MgO nanoparticles with different MgO contents. It can be seen that the MEA performance is obviously improved after the formation of porous anodic CLs. The maximum power densities are 30.6, 34.6, 37.2, 37.0 mW cm^{-2} for the MEAs with porous anodic CLs prepared by removal of 0, 10, 15 and 20 wt.% MgO nanoparticles, respectively. The MEA performance reaches a stable value after the addition of ca. 15–20 wt. % MgO as sacrifice templates. Fig. 2(B) demonstrates the effect of porous anodic MPLs prepared by removal of MgO nanoparticles with different MgO contents. It can be seen that the maximum power densities are 34.4 and 35.9 mW cm^{-2} for the MEAs with anodic porous MPLs prepared by removal of 10 and 20 wt. % MgO nanoparticles, respectively. There is no big difference in cell performance between the MEAs with the addition of 10 and 20 wt. % MgO into MPLs. The lower porosity required for sufficient

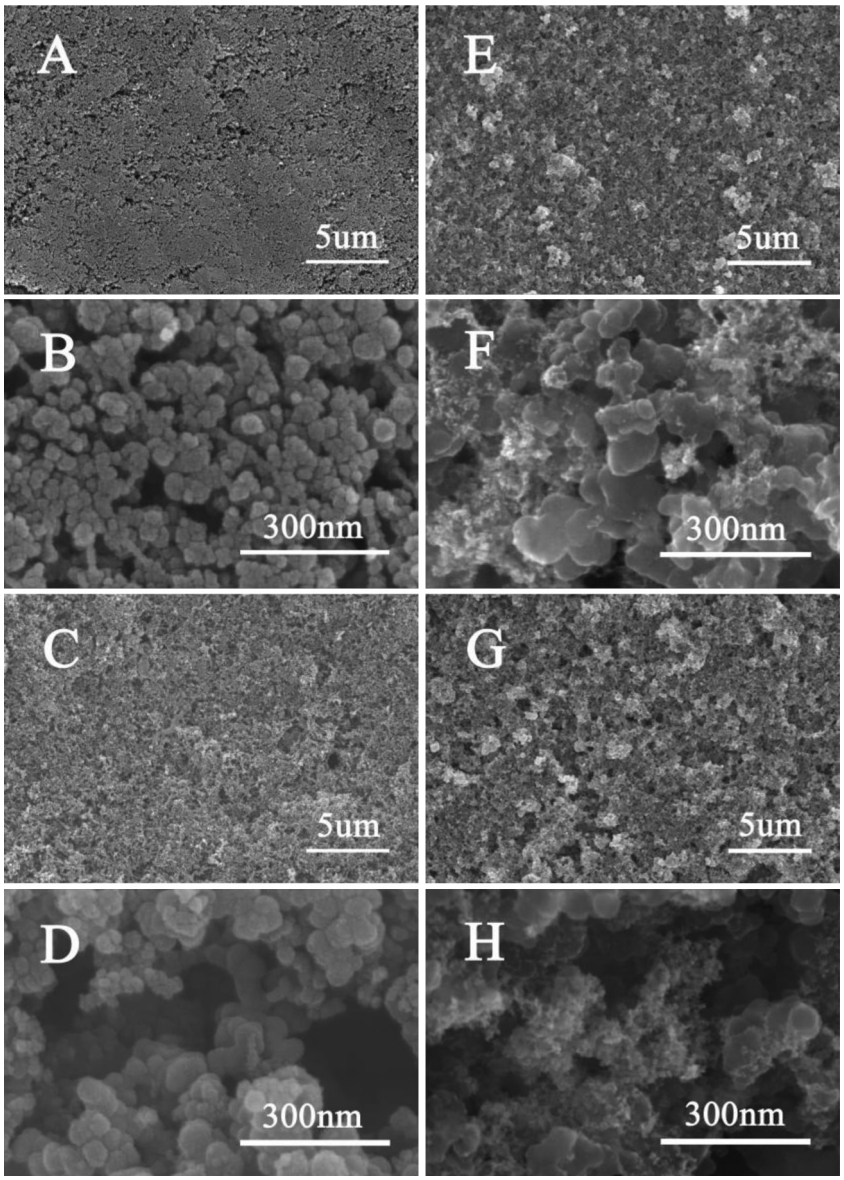

Fig. 1. SEM images of conventional MPL (A, B), porous MPL (C, D) after removal of 20 wt. % MgO particles, conventional CL (E, F) and porous CL (G, H) after removal of 20 wt. % MgO particles.

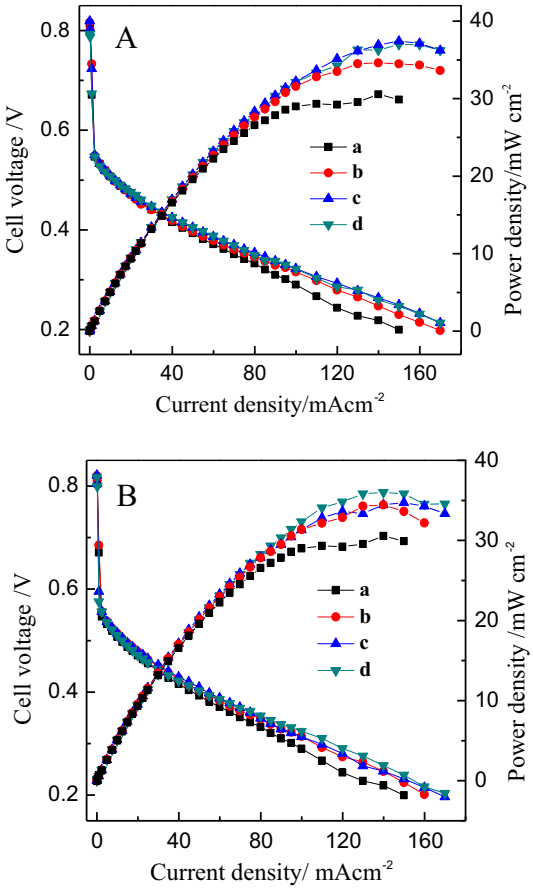

Fig. 2. Polarization curves of the DMFCs with porous CLs (A) and porous MPLs (B) formed by removal of MgO nanoparticles with its content of 0 (a), 10% (b), 15% (c) and 20% (d) and with a PtRu loading of 2 mg cm^{-2}.

promotion of cell performance may be ascribed to the lower thickness and mass transform resistance of the anodic MPLs than that of CLs.

In general, the catalyst loadings used in a passive DMFC are about 10 times higher than that in a H_2–O_2 PEMFC. Therefore, it is urgent to reduce the catalyst loadings within the CLs of a DMFC for practical application. In this paper, we explored the maximum savings of catalyst loading based on the better performance of the MEAs with porous CLs and porous MPLs. Fig. 3 shows the polarization curves of the MEAs with conventional anodic structure at a PtRu loading of 2 mg cm^{-2} and with only porous CLs, only porous MPLs and with both porous MPLs and CLs at different PtRu loadings. As seen from Fig. 3 and Table 1, for the MEA with porous CLs and porous MPLs, the performance of the MEA with a PtRu loading of 1.5 mg cm^{-2} could exceed that for the conventional one with a PtRu loading of 2.0 mg cm^{-2}. To combine the positive effects of porous CLs and porous MPLs, the polarization curves of the MEAs with pores formed by the removal of 20 wt. % MgO nanoparticles both within the MPLs and CLs are shown in Fig. 3(C). At a PtRu loading of 2.0 mg cm^{-2}, the maximal power density of an MEA with simultaneous formation of pores on CL and MPL is 43.7 mW cm^{-2}. When the PtRu loading is reduced to 1.0 mg cm^{-2}, the power density of porous MEA still reaches a peak value of 32.8 mW cm^{-2}, which is slightly higher than that of a conventional MEA with a PtRu loading of 2.0 mg cm^{-2}. Obviously, the formation of pores within both MPL and CL by removal of MgO nanoparticles leads to a significant reduction in PtRu loading, but without a DMFC performance loss. Furthermore, in the low current density region, the four passive

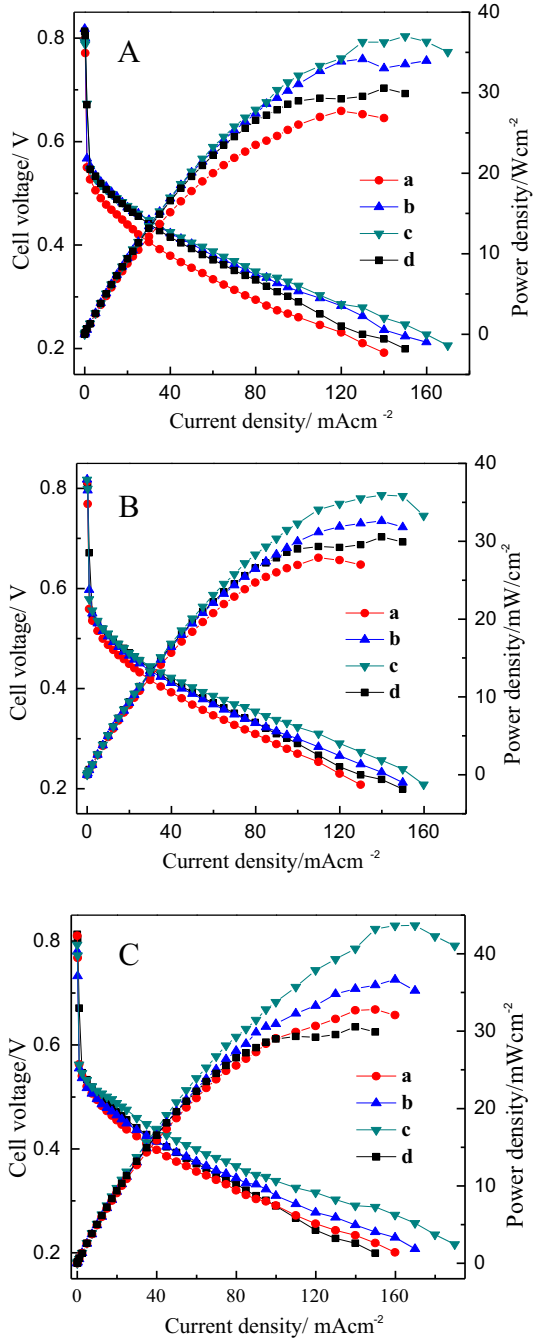

Fig. 3. Polarization curves of the MEAs with only porous CL (A), only porous MPL (B) and both porous MPL and CL (C) at PtRu(1:1) loadings of 1.0 (a), 1.5 (b) and 2.0 mg cm^{-2} (c), respectively. The MEA with conventional anodic structure at a PtRu loading of 2 mg cm^{-2} (d) is also given for a comparison.

Table 1
Maximal power densities of the MEAs with the anodes without and with porous structures formed by the removal of 20 wt. % MgO nanoparticles (mW cm^{-2}).

PtRu loading/mg cm^{-2}	1.0	1.5	2.0
Conventional	24.0	27.5	30.6
Porous CL	27.7	34.2	37.0
Porous MPL	27.9	32.6	35.9
Porous MPL and CL	32.8	36.7	43.7

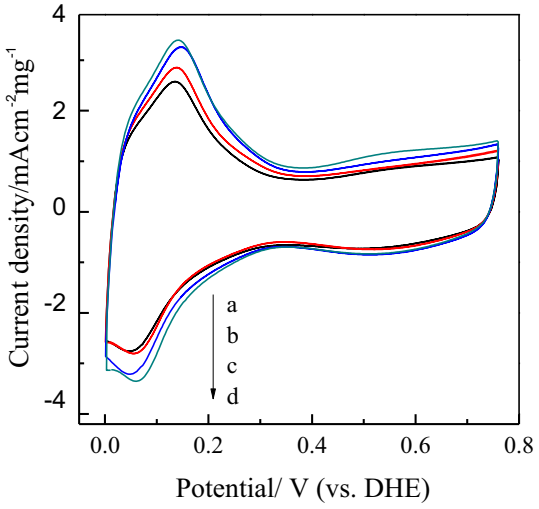

Fig. 4. CVs of a conventional anode (a) and the anodes with porous CL formed by removal of 10 wt. % (b) and 20 wt. % MgO nanoparticles (c) as well as with both porous CL and MPL formed by removal of 20 wt. % MgO nanoparticles (d) with a PtRu(1:1) loading of 2.0 mg cm^{-2}.

DMFCs exhibit a similar kinetic and ohmic polarization behavior. However, at the high current density region, a fast decay in cell's voltage for the conventional MEA is observed, strongly suggesting that the mass transfer on the anode can be greatly improved for the MEAs with porous anodic structure.

To explore the possible reasons for the improved cell performance of the DMFCs with anodic porous MPLs and CLs, CV and EIS measurements were conduced. Fig. 4 presents the CVs of the anodes for the four MEAs with different anodic structures with a PtRu loading of 2.0 mg cm^{-2}. The redox peaks in the potential range of 0.05–0.4 V can be attributed to the H adsorption/desorption on the surface of PtRu nanoparticles. The calculated ECSAs for the anodes with porous CLs formed by 10 and 20 wt. % MgO particles are 33.81 and 39.38 $m^2\ g^{-1}$, respectively; which are much higher than that of conventional anode with an ECSA of 26.34 $m^2\ g^{-1}$, indicative of an obvious improvement in catalyst utilization for the porous CLs. The simultaneous formation of porous MPL and CL of MEA leads to a further increase in ECSA to 40.24 $m^2\ g^{-1}$, which is slightly higher than that of the anode with only porous CL.

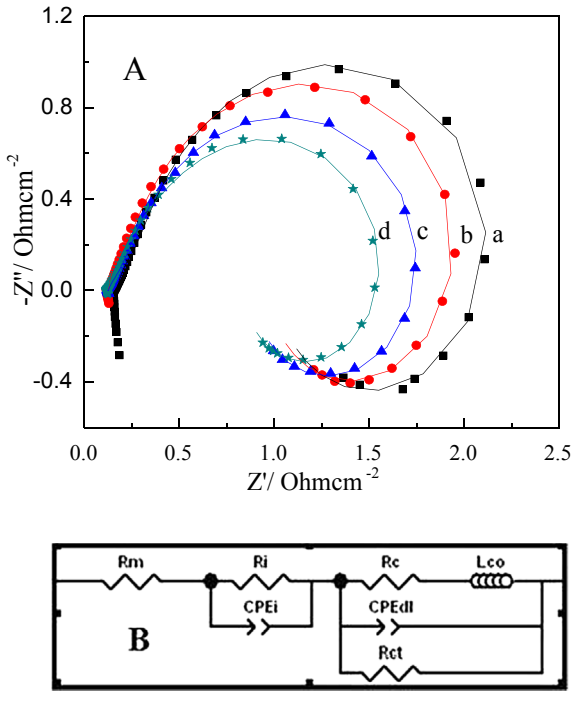

Fig. 5. Experimental EIS spectra (A) and equivalent circuit (B) of a conventional anode (a) and porous anodes with porous CL formed by removal of 10 wt. % (b) and 20 wt. % MgO nanoparticles (c) as well as with both porous CL and MPL formed by removal of 20 wt. % MgO nanoparticles (d) with a PtRu(1:1) loading of 2.0 mg cm^{-2} and at a given DC potential of 0.4V/DHE.

Fig. 5(A) presents experimental EIS spectra of the anodes of the MEAs with conventional and porous anodes. An equivalent circuit model is shown in Fig. 5(B). In this model, the constant phase elements (CPE) are used to replace ideal capacitors and to account for the non-uniform structure of the related electrodes [31]. Thus, the physical meanings of each element employed in the equivalent circuit model (Fig. 5(B)) are as follows:

R_m stands for the resistance of the membrane;

The anode-membrane interface contribution contains CPE_i and R_i, which describe the capacitive behavior and contact resistance between the membrane and CL, respectively;

R_{ct} is the charge-transfer resistance of the anodic reaction;
CPE_{dl} describes the capacitive behavior of the anode with roughness of the CL and non-uniform catalyst distribution;
L_{co} means that the current signal follows voltage perturbation with a phase-delay due to slowness of CO desorption on the anode;
R_c denotes the resistance of the solid phase in anodic catalytic layer.

The fitted parameters are provided in Table 2. As observed, the values of *R*c, *L*co and *R*ct of the anodes become smaller with the increase in MgO content added into the anodes, which could explain the improved performance of the DMFC with porous anodic CLs. Moreover, it is noticeable that the *R*ct value of the anodes with both porous MPL and CL is obviously smaller than that with only porous CL while keeping the same 20 wt. % MgO content for pore-forming. Obviously, the enhanced performance of the DMFCs with the porous anodic structures can be ascribed to an increase in catalyst utilization and to a decrease in charge transfer resistance.

To determine the energy efficiency of the DMFCs, transient discharging curves of the two passive DMFCs with both porous anodic MPL and CL formed by removal of 20 wt. % MgO particles and with conventional anodic structure at a constant voltage of 0.35 V are shown in Fig. 6. It is clear that the discharge current of the two DMFCs, both fueled with 5.0 mL of 3 M methanol, decays

Table 2
Fitted parameters for the CPE-based equivalent circuit model for the different anodes of the passive DMFCs operating at 0.4V/DHE.

Parameter	Conventional	Porous CL formed with 10 wt. % MgO	Porous CL formed with 20 wt. % MgO	Porous MPL and CL formed with 20 wt. % MgO
R_m (Ohm cm^2)	0.173	0.128	0.125	0.118
R_i (Ohm cm^2)	0.125	0.112	0.108	0.082
CPE_i-T(F cm^{-2})	0.622	0.560	0.450	0.380
CPE_i-P	0.860	0.761	0.681	0.653
R_c (Ohm cm^2)	1.162	1.122	1.065	1.020
L_{co} (H cm^{-2})	11.51	11.23	10.30	9.48
CPE_{dl}-T(F cm^{-2})	0.816	0.822	0.828	0.830
CPE_{dl}-P	0.915	0.918	0.920	0.938
R_{ct} (Ohm cm^2)	2.285	2.156	1.822	1.545

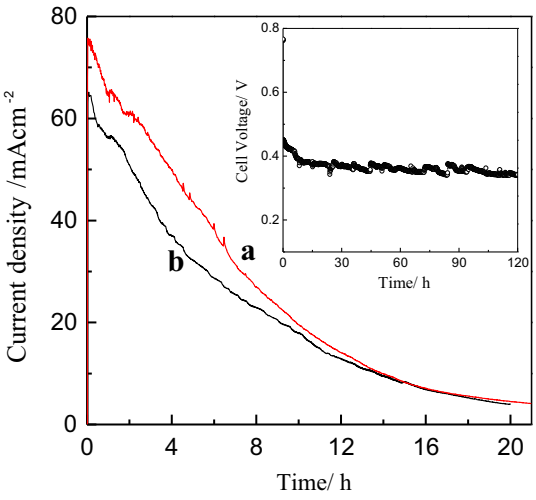

Fig. 6. Transient discharging curves of the two passive DMFCs with both porous MPL and CL formed by removal of 20 wt. % MgO particles (a) and with conventional anodic structure (b) at a constant voltage of 0.35 V with a start for the DMFCs to be fueled with 5 mL of 3 mol L^{-1} methanol. Insert: the stability test of the DMFC with both porous MPL and CL formed by removal of 20 wt. % MgO nanoparticles.

with time, probably due to the fact that the rate of methanol transfer from the reservoir to the anode catalyst layer is lower than that of methanol consumed on the catalyst layer, and that the methanol concentration continuously decreased during the discharging. However, the discharge current of the DMFC with porous anodic MPL and CL is slightly higher than that with conventional MPL and CL in the first 12 h, suggesting that the presence of porous anode promotes the methanol transport from the reservoir to the anodic CL. For the two passive DMFCs, energy efficiency can be calculated from two curves in Fig. 6. The calculated energy efficiencies are 24.9% and 21.6% for the DMFCs with both porous MPL and CL and with conventional one, respectively; suggesting that an increased methanol utilization is obtained for the passive DMFC with porous anodic structure. To investigate the durability of a passive DMFC with porous anodic structure, the DMFC was continuously discharged at a constant current density of 40 mA cm^{-2} by continuously feeding 3 M methanol. As seen in the insert of Fig. 6, a stable cell performance was observed for about 120 h operation, confirming that the stability of such a DMFC is good for the practical application with an improved cell performance.

4. Conclusions

In summary, the simple addition of magnesium oxide nanoparticles as a sacrificial pore-former into the anodic catalytic layer and micro-porous layer of a DMFC leads to a significant increase in catalyst utilization and a decrease in charge-transfer resistance of the anodic reaction, thus greatly improved the DMFC's performance and allowed a dramatic reduction in noble metal loading within the membrane electrode assembly. The current work provides a promising way for the decrease of noble metal loadings for fuel cells' applications.

Acknowledgments

We would like to thank the National Basic Research Program of China (973 Program, 2012CB932800), The Nature Science Foundation of China (21276158, 21373256), Shanghai Science and Technology Committee (11DZ1200400, 12ZR1431200) and the Knowledge Innovation Engineering of the Chinese Academy of Sciences (12406, 124091231) for support to this work.

References

[1] A.S. Aricò, S. Srinivasan, V. Antonucci, Fuel Cells 1 (2001) 133–161.
[2] C.M. Miesse, W.S. Jung, K.-J. Jeong, J.K. Lee, J. Lee, J. Han, S.P. Yoon, S.W. Nam, T.-H. Lim, S.-A. Hong, J. Power Sources 162 (2006) 532–540.
[3] H. Tang, S. Wang, M. Pan, R. Yuan, J. Power Sources 166 (2007) 41–46.
[4] S. Litster, G. McLean, J. Power Sources 130 (2004) 61–76.
[5] J.T. Gostick, M.A. Ioannidis, M.W. Fowler, M.D. Pritzker, Electrochem. Commun. 11 (2009) 576–579.
[6] W. Hartmut, F. Andreas, Z. Ralf, EP 0,797,265, 1997.
[7] S. Wang, G.Q. Sun, G. Wang, Z. Zhou, X. Zhao, H. Sun, et al., Electrochem. Commun. 7 (2005) 1007–1012.
[8] H. Tang, W.M. Pan, S.P. Jiang, Y. Ruan, Electrochim. Acta 52 (2007) 3714–3718.
[9] F. Liu, C.-Y. Wang, Electrochim. Acta 52 (2006) 1417–1425.
[10] Q. Mao, G. Sun, S. Wang, H. Sun, G. Wang, Y. Gao, et al., Electrochim. Acta 52 (2007) 6763–6770.
[11] R. O'Hayre, S.-W. Cha, W. Colella, F.-B. Prinz, Fuel Cell Fundamentals, second ed., Willy, 2009, pp. 83–98.
[12] Z. Wei, S. Wang, B. Yi, J. Liu, L. Chen, W. Zhou, W. Li, Q. Xin, J. Power Sources 106 (2002) 364–369.
[13] T.V. Reshetenko, H.-T. Kim, H.-J. Kweon, Electrochim. Acta 53 (2008) 3043–3049.
[14] W. Zhang, P.N. Pintauro, ChemSusChem 4 (2011) 1753–1757.
[15] M. Chisaka, H. Daiguji, Electrochem. Acta 51 (2006) 4828–4833.
[16] Y.-H. Cho, N. Jung, Y.S. Kang, D.Y. Chung, J.W. Lim, H. Choe, Y.-H. Cho, Y.-E. Sung, Int. J. Hydrogen Energy 37 (2012) 11969–11974.
[17] T.V. Reshetenko, H.-T. Kim, H.-J. Kweon, J. Power Sources 171 (2007) 433–440.
[18] G.-C. Liu, Y.-T. Wang, J. Zhang, M. Wang, C.-J. Zhang, X.-D. Wang, J. Chem. Technol. Biotechnol. 88 (2013) 818–822.
[19] Y. Song, Y. Wei, H. Xu, M. Williams, Y. Liu, L.J. Bonville, H.R. Kunz, J.M. Fenton, J. Power Sources 141 (2005) 250–257.
[20] P. Wu, B. Li, H. Du, L. Gan, F. Kang, Y. Zeng, J. Power Sources 192 (2009) 324–329.
[21] G. Wang, G. Suna, Q. Wang, S. Wang, J. Guo, Y. Gao, Q. Xin, J. Power Sources 180 (2008) 176–180.
[22] D. You, Y. Lee, H. Cho, J.-H. Kim, C. Pak, G. Lee, K.-Y. Park, J.-Y. Park, Int. J. Hydrogen Energy 36 (2011) 5096–5103.
[23] Y. Lee, T.K. Kim, Y.S. Choi, Fuel Cells 13 (2013) 173–180.
[24] H. Liu, C. Song, L. Zhang, J. Zhang, H. Wang, D.P. Wilkinson, J. Power Sources 155 (2006) 95–110.
[25] Z. Liu, L. Yang, Z. Mao, W. Zhuge, Y. Zhang, L. Wang, J. Power Sources 157 (2006) 166–176.
[26] N. Yousfi-Steiner, Ph Moçotéguy, D. Candusso, D. Hissel, J. Power Sources 194 (2009) 130–145.
[27] M.C. Tucker, M. Odgaard, P.B. Lund, S.Y. -Andersen, J.O. Thomasa, J. Electrochem. Soc. 152 (2005) A1844–A1850.
[28] T. Yuan, Z. Zou, M. Chen, Z. Li, B. Xia, H. Yang, J. Power Sources 192 (2009) 423–428.
[29] A.S. Bauskara, C.A. Rice, Electrochim. Acta 62 (2012) 36–41.
[30] K.T. Jeng, C.C. Chien, N.Y. Hsu, W.M. Huang, S.D. Chiou, S.H. Lin, J. Power Sources 164 (2007) 33–41.
[31] N.Y. Hsu, S.C. Yen, K.T. Jeng, C.C. Chien, J. Power Sources 142 (2005) 169–176.